Bioengineered

ISSN: 2165-5979 (Print) 2165-5987 (Online) Journal homepage: https://www.tandfonline.com/loi/kbie20

Quantitative analysis of multiple biokinetic models using a dynamic water phantom: A feasibility study

Fu-Tsai Chiang, Pei-Jung Li, Shih-Ping Chung, Lung-Fa Pan & Lung-Kwang Pan

To cite this article: Fu-Tsai Chiang, Pei-Jung Li, Shih-Ping Chung, Lung-Fa Pan & Lung-Kwang Pan (2016) Quantitative analysis of multiple biokinetic models using a dynamic water phantom: A feasibility study, Bioengineered, 7:5, 304-313, DOI: 10.1080/21655979.2016.1197738

To link to this article: https://doi.org/10.1080/21655979.2016.1197738

BIOENGINEERED
2016, VOL. 7, NO. 5, 304–313
http://dx.doi.org/10.1080/21655979.2016.1197738

Taylor & Francis
Taylor & Francis Group

RESEARCH PAPER

Quantitative analysis of multiple biokinetic models using a dynamic water phantom: A feasibility study

Fu-Tsai Chiang[a,b], Pei-Jung Li[c], Shih-Ping Chung[a,d], Lung-Fa Pan[a,e], and Lung-Kwang Pan[a]

[a]Graduate Institute of Radiological Science, Central Taiwan University of Science and Technology, Takun, Taiwan, ROC; [b]Department of Orthopedic Surgery, Taichung Armed Forces General Hospital, Taichung, Taiwan, ROC; [c]Department of Nuclear Medicine, Changhua Christian Hospital, Taiwan, ROC; [d]Department of Nuclear Medicine, Buddhist Tzu Chi General Hospital, Taichung Branch, Taiwan, ROC; [e]Department of Cardiology, Taichung Armed Forces General Hospital, Taiwan, ROC

ABSTRACT

This study analyzed multiple biokinetic models using a dynamic water phantom. The phantom was custom-made with acrylic materials to model metabolic mechanisms in the human body. It had 4 spherical chambers of different sizes, connected by 8 ditches to form a complex and adjustable water loop. One infusion and drain pole connected the chambers to an auxiliary silicon-based hose, respectively. The radio-active compound solution (TC-99m-MDP labeled) formed a sealed and static water loop inside the phantom. As clean feed water was infused to replace the original solution, the system mimicked metabolic mechanisms for data acquisition. Five cases with different water loop settings were tested and analyzed, with case settings changed by controlling valve poles located in the ditches. The phantom could also be changed from model A to model B by transferring its vertical configuration. The phantom was surveyed with a clinical gamma camera to determine the time-dependent intensity of every chamber. The recorded counts per pixel in each chamber were analyzed and normalized to compare with theoretical estimations from the MATLAB program. Every preset case was represented by uniquely defined, time-dependent, simultaneous differential equations, and a corresponding MATLAB program optimized the solutions by comparing theoretical calculations and practical measurements. A dimensionless agreement (AT) index was recommended to evaluate the comparison in each case. ATs varied from 5.6 to 48.7 over the 5 cases, indicating that this work presented an acceptable feasibility study.

ARTICLE HISTORY
Received 18 March 2016
Revised 08 May 2016
Accepted 1 June 2016

KEYWORDS
biokinetic model; dynamic phantom; multiple compartments; Tc-99 m

Introduction

In this study, multiple biokinetic models were quantitatively analyzed using a dynamic water phantom. Dynamic phantoms are widely applied in medical fields to simulate metabolic mechanisms in the human body. Most phantoms are specially designed either to survey the imaging system in order to increase diagnostic accuracy or to evaluate radioactive dosage for quality assurance. Phantoms are more convenient in these contexts compared to the human body because of the high reproducibility of tests and easy manipulation in manual operations. For example, the dynamic cardiac phantom known as ECT/DY-CAR/P (Dynamic Cardiac Phantom™) was designed to provide gated cardiac imaging, measure uniformity of myocardial wall, and assist in clinical research.[1] Similarly, the dynamic thorax phantom, model 008 A (Tissue Simulation & Phantom Technology, CIRS) was designed to verify image acquisition, aid in treatment planning, and improve dose delivery systems.[2] One custom-made dynamic lung and liver phantom was designed to mimic real 3-dimensional motions in order to suppress residual motions occurring in 4-dimensional PET scans.[3] Some phantoms are also custom-made to fulfill their special needs in either research or academic field.[4-7] However, few phantoms have explored multi-compartment biokinetic models, because the complicated calculations required to solve the biokinetic models and the time-consuming verifications of the obtained solutions have impeded investigations over the past decade. In order to quantitatively analyze the

CONTACT Lung-Kwang Pan lkpan@ctust.edu.tw Dept. Of Med. Imag & Radio. Sci., Central Taiwan University of Science and Technology, Takun, Taichung, Taiwan, R.O.C.

Color versions of one or more of the figures in the article can be found online at www.tandfonline.com/kbie.

biokinetic models for metabolic mechanisms, a group of time-dependent, simultaneous differential equations with unique definitions for corresponding compartments must be arranged properly according to the guidelines set forth in the International Commission on Radiation Protection (ICRP-30 or the ICRP-100 reports);[8,9] furthermore, each compartment must be assigned to represent either a dominant organ or the summarized metabolic system in the model calculation in order to derive a convincing result.

In this work, a custom-made water phantom was designed to verify the time-dependent biokinetic model analysis for multiple metabolic mechanisms in the human body. The phantom could be easily preset to satisfy the definitions of the various biokinetic models, 5 of which were tested in this work. Radioactive Tc-99m-MDP labeled solutions originally filled the phantom's 4 chambers to be replaced gradually with infused fresh water to simulate the metabolic system in a real human body. The infused water flow rate could be adjusted precisely using a medical infusion pump. A gamma camera constantly monitored the radioactive concentration inside each chamber, and the acquired counts per pixel of targets regions were recorded, normalized, and analyzed using a self-developed MATLAB program. This work recommended a dimensionless agreement (AT) to quantify the correlation between the practical measurements and theoretical estimations of every case. The feasibility study verified that the dynamic water phantom was easily assembled and that the analysis correlated to either the theoretical calculation or the practical evaluation. Ultimately, the phantom proved successful in multiple applications representing the different biokinetic models.

Materials and method

Dynamic water phantom

The phantom was assembled from 2 independent acrylic cubes. Each cube (400×330×95 mm^3, 12.6 kg) was machined and milled to contain 4 hemi-spherical chambers connected by ditches. Fig. 1 shows the 2 halves of each acrylic cube: (A) top view of the assembled phantom, (B) split into the completed halves, (C) close-up view of the valve pole in the middle of the ditch between the spherical chambers, and (D) spherical chambers labeled as regions of interest (ROI) (1)–(4). As Fig. 1 shows, ROI (1) (r = 4 cm, 268 cc) was set on the top, with ROI (2) (r = 7 cm, 1437 cc) on the left and ROI (4) (r = 6 cm, 905 cc) on the right. ROI (3) was the smallest region (r = 2 cm, 34 cc). A tight rubber ring around the perimeter of the spherical chambers and ditches established water-proofing when the 2 half cubes were put together. Only one infusion or drain port was kept on top of ROI (1) or beneath ROI (3) to maintain balance. A valve was inserted in middle of every ditch, and the valves were easily loosened and tightened by manipulating the pole. Many kinds of water loops could be created by adjusting the 8 valves among the 4 ROIs; in fact, more than 50 combinations were possible. The phantom with ROI (1) on top was defined as "model A," and "model B" had ROI (3) on top and was easily overturned during use. This work measured and verified 3 cases in model A: (1) single path 1-4-3, (2) double path 1-4-3 and 1–2, (3) full release; and two cases in model B: (4) 3-2-1 and 4–1 and (5) full release.

Biokinetic model

Various biokinetic models can be defined according to the configuration of compartments shown as ROIs in Fig. 2 (A) Model A, and (B) model B. The phantom models the different metabolic systems in human body, and each compartment can represent a dominant organ like a thyroid, liver, or kidney, or a summarized metabolic system like the whole body or body fluids.[8] The phantom can be easily changed from model A to model B by overturning it, as Fig. 1 shows. Equations 1–4 and 5–9 are 2 groups of simultaneous differential equations that describe the time-dependent correlation among the compartments' radio-activate solutions.

Model A

$$\frac{dN_1}{dt} = -(\lambda_R + \lambda_{12} + \lambda_{13} + \lambda_{14})N_1 \quad (1)$$

$$\frac{dN_2}{dt} = \lambda_{12}N_1 - (\lambda_R + \lambda_{23} + \lambda_{25})N_2 + \lambda_{23}N_3 \quad (2)$$

$$\frac{dN_3}{dt} = \lambda_{13}N_1 + \lambda_{23}N_2 - (\lambda_R + \lambda_{23} + \lambda_{34} + \lambda_{35})N_3 + \lambda_{34}N_4 \quad (3)$$

$$\frac{dN_4}{dt} = \lambda_{14}N_1 + \lambda_{34}N_3 - (\lambda_R + \lambda_{34} + \lambda_{45})N_4 \quad (4)$$

Figure 1. The 2 halves of each acrylic cube: (A) top view of the assembled phantom, (B) split into the completed halves, (C) close-up view of the valve pole in the middle of the ditch between the spherical chambers, and (D) spherical chambers labeled as regions of interest (ROI) (1)–(4).

Model B

$$\frac{dN_5}{dt} = -(\lambda_R + \lambda_{25} + \lambda_{35} + \lambda_{45})N_5 \quad (5)$$

$$\frac{dN_4}{dt} = -(\lambda_R + \lambda_{14} + \lambda_{34})N_4 + \lambda_{45}N_5 \quad (6)$$

$$\frac{dN_3}{dt} = -(\lambda_R + \lambda_{13} + \lambda_{23} + \lambda_{34})N_3 + \lambda_{35}N_5 \quad (7)$$

$$\frac{dN_2}{dt} = -(\lambda_R + \lambda_{23} + \lambda_{12})N_2 + \lambda_{25}N_5 \quad (8)$$

$$\frac{dN_1}{dt} = -(\lambda_R + \lambda_{10})N_1 + \lambda_{12}N_2 + \lambda_{13}N_3 + \lambda_{14}N_4 \quad (9)$$

The terms N_i and λ_{ij} represent, respectively, the time-dependent quantity of the specific radionuclide and the biological decay constant ($\lambda_{ij} = I_{ij} \cdot \ln 2 / T_{i(1/2)}(\text{bio})$), where I_{ij} is the branching ratio of the infused water from the ith into the jth compartment, $T_{i(1/2)}(\text{bio})$ is the biological half-life of the ith compartment, and λ_R is the radiological decay constant of the specific radionuclide, which is Tc-99 m in this work. In model A, only one input was provided from Input (0) to ROI (1), before splitting among ROIs (2), (3), and (4); therefore I_{01} is 1.00, as is the sum of I_{12}, I_{13}, and I_{14} (i.e. sum = 1.00). Meanwhile, in model B, the water was split into 3 paths in the beginning, making the sum of I_{45}, I_{35}, and I_{25} equal 1.00 in the model calculation. The results can be calculated and plotted using a program developed in MATLAB to find an optimal solution to equations 1–4 or 5–9 and to plot the time-dependent simultaneous differential equations to verify the specific biokinetic model.

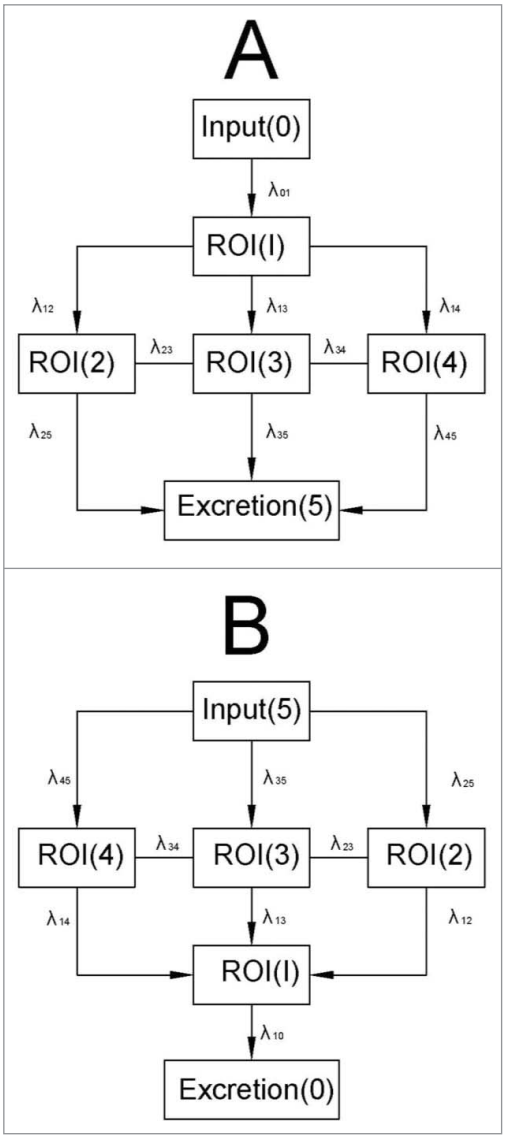

Figure 2. Various biokinetic models can be defined according to the configuration of compartments shown as ROIs in (A) Model A, and (B) model B.

Gamma camera survey

This study used 122.1±59.2 MBq of Tc-99 m labeled methylene diphosphonate (MDP) in 5 measurements.[10] The activated solution was mixed homogeneously with 2800 cc deionized water and infused into the dynamic phantom before measurement. A medical infusion pump (IV pump, Hospira plum XL series) was connected to the infusion port (see Fig 1D, at the top of the ROI (1)) with a silicon-based 1-m hose, and the drain port was connected to another 1.2-m hose (see Fig 1D, beneath ROI (3)). The crucial factor in this arrangement was that the maximum height of the drain hose needed to maintain the same height as the infusion port; this was essential to maintain the water balance inside the phantom.

An initial time measurement was recorded when the fresh water was infused by the IV pump into the phantom. The theoretical biological half-life of every spherical chamber was defined as half the volume divided by the feed-water infusion rate. For example, the biological half-life of chamber 1 (ROI (1)) was 26.8 min. when the feed-water infusion rate was set at 5 cc/min (268[cc] / 2 / 5 [cc·min^{-1}] = 26.8 [min]). Furthermore, λ_{12} for model A (see Eqs. 1–4) could be determined to be 0.0259 [min^{-1}] (ln2/26.8 = 0.0259) when I_{12} was 1.00. The λ_R is 0.001925 [min^{-1}] (ln2/360 = 0.001925) because the radiological half-life of Tc-99 m is 360 min. However, the practical biological half-life for every ROI was still allowed to revise in order to satisfy the real measured data in the gamma camera image acquiring system.

The gamma camera (Infinia Hawkeye 4) was located at the Department of Nuclear Medicine in Buddhist Tzu Chi General Hospital, Taichung. The camera's 2 NaI (54×40×0.95 cm^3) plate detectors were positioned at 10 cm in front of and 12 cm behind the phantom during scanning. Each plate was connected to a group of 53×3 in- and 6×1.5 in-diameter photo multiplier tubes (PMT) in order to record data. The two detectors captured about 70% of the emitted gamma rays behind the low energy high resolution (LEHR) collimator.[11,12] Figure 3 depicts the arrangement of the water phantom between the gamma camera's 2 NaI plates. As previously noted, the container for holding the draining water was kept at the same height as the top of the phantom in order to assure the water balance.

Data collection and measurement were initiated when the IV pump began to feed in the water. The scan protocol took 5 min collection every half hour for 3 h and proceeded as follows: vertical position, energy peak of 140 keV (window: 20%), LEHR collimator, 128×128 matrix, and static scan in every practical measurement. Ultimately, 7 data sets were obtained and analyzed for each case. Figure 4 presents the 7 imaging plots from the gamma camera. The images were obtained in a preliminary survey that was performed using a similar protocol. Figure 4 clearly shows that the phantom was measured in model A, as the darkest spot was recorded in ROI (1) on the right side of the scanned images. In addition, the ROIs were marked and recorded by well-trained radiologist

Figure 3. The arrangement of the water phantom between the gamma camera's 2 NaI plates. As previously noted, the container for holding the draining water was kept at the same height as the top of the phantom in order to assure the water balance.

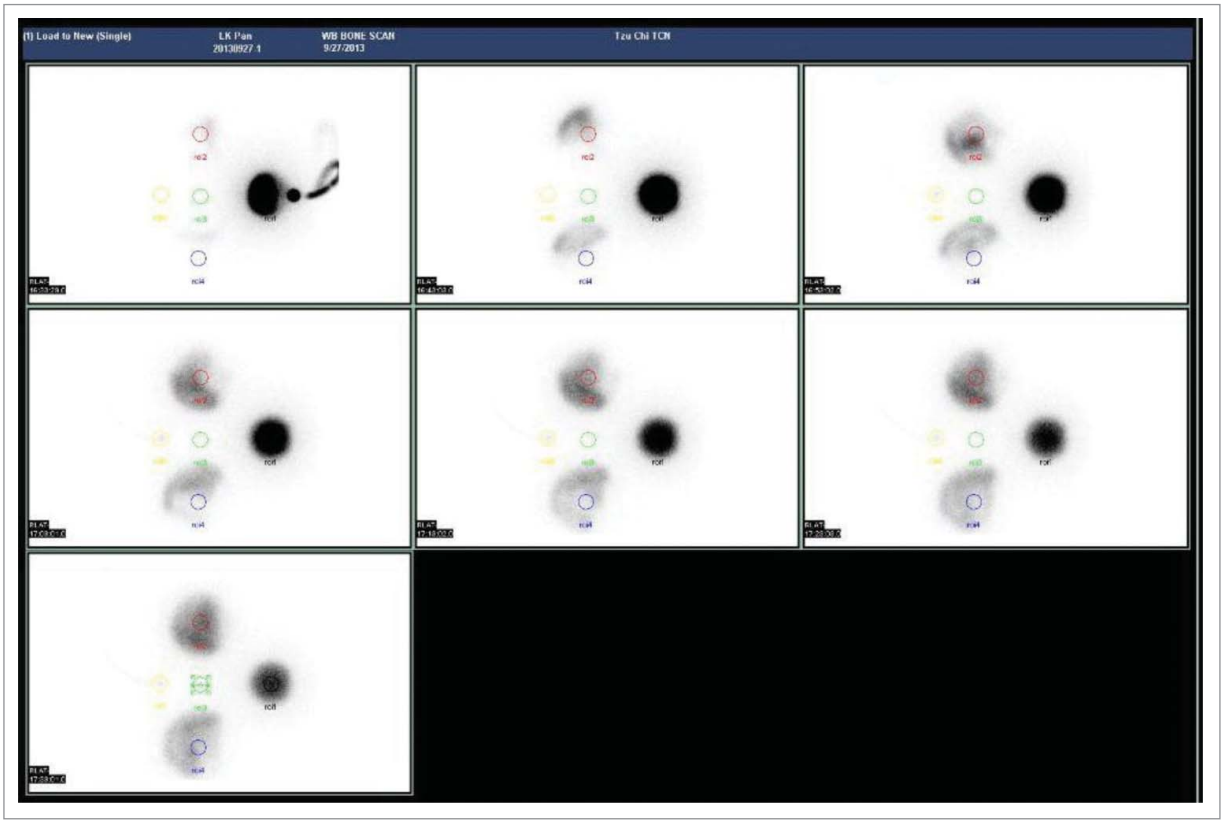

Figure 4. The 7 imaging plots from the gamma camera. The images were obtained in a preliminary survey that was performed using a similar protocol. The phantom was measured in model A, as the darkest spot was recorded in ROI (1) on the right side of the scanned images. In addition, the ROIs were marked and recorded by well-trained radiologist directly from the clinical monitor beside the gamma camera facility.

directly from the clinical monitor beside the gamma camera facility.

Results

Biokinetic models

This study surveyed and analyzed 5 cases, 3 using model A single path 1-4-3, double path 1-4-3 and 1–2, and full release and 2 using model B double path 3-2-1 and 4–1, and full release. Figure 5 shows the results derived from the MATLAB calculation in the form of 4 continuous lines, as well as the normalized data set in 4 groups of separated dots. Table 1 shows all the derived biological half-lives and variables for the simultaneous differential equations used in this work. The calculation results represent theoretical estimations of the time-dependent

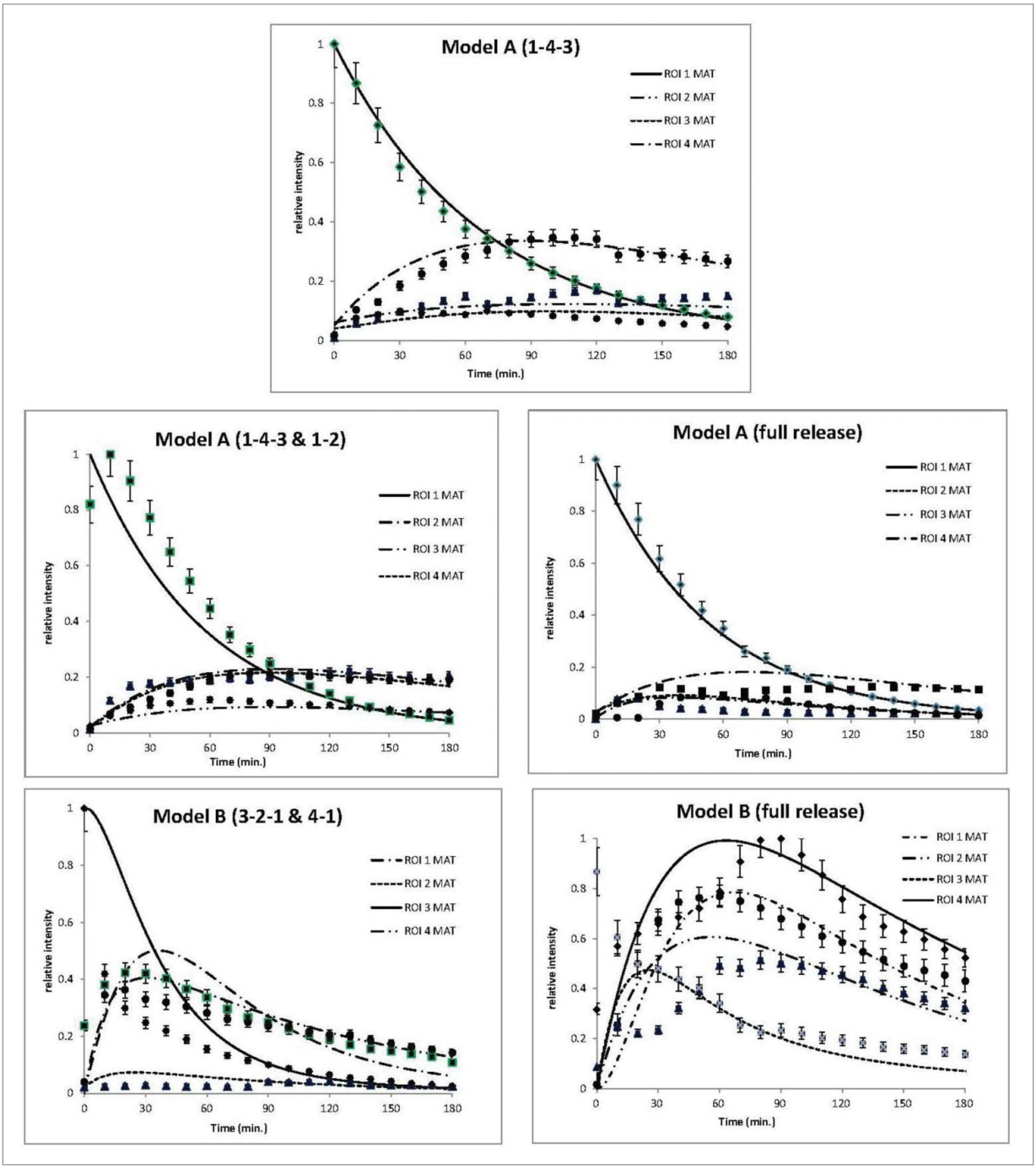

Figure 5. The results derived from the MATLAB calculation in the form of 4 continuous lines, as well as the normalized data set in 4 groups of separated dots.

Table 1. The derived biological half-lives and variables for simultaneous time-dependent, differential equations as adopted in this work. The calculation results are theoretical estimations of the time-dependent quantity of Tc-99 m in various compartments for 5 cases according to the MATLAB calculation. Additionally, the decay constant of radiological half-life of Tc-99 m is indicated as $T_{1/2}$(R) which is 360 min.

	Model A			Model B		
	Case 1	Case 2	Case 3	Case 4	Case 5	Theoretical Derivation [min]
$T1_{/2}$(R)	360	360	360	360	360	360
$T_{1/2}$(ROI 1)	54	45	41	21	24	268/2/5=26.8
$T1_{/2}$(ROI 2)	290	110	18	85	96	1437/2/5=143.7
$T_{1/2}$(ROI 3)	8	31	7.3	18	12	34/2/5=3.4
$T1_{/2}$(ROI 4)	88	95	87	88	115	905/2/5=90.5
i_{10}	—	—	—	1.00	1.00	
i_{12}	0.14	0.42	0.36	0.08	0.24	
i_{13}	0.14	0.17	0.34	0.42	0.42	
i_{14}	0.72	0.41	0.30	0.54	0.34	
I_{23}	0.70	0.98	0.40	0.40	0.76	
I_{25}	0.30	0.02	0.06	0.27	0.19	
I_{32}	—	—	—	0.46	0.40	
I_{34}	—	—	—	0.04	0.09	
I_{35}	0.25	1.00	1.00	0.46	0.62	
I_{43}	0.99	0.98	0.41	0.40	0.70	
I_{45}	0.01	0.02	0.59	0.27	0.19	

quantity of Tc-99 m in various compartments for all cases, as determined by the MATLAB calculation. The decay constant of Tc-99m's radiological half-life is indicated as $T_{1/2}$(R), which is 360 min. Most of the ROIs' derived biological half-lives did not agree the theoretical ones, which were simply calculated as half the specific ROI volume divided by the feed water flow rate, which was 5 cc/min.

Case 2 in ROI (3) and case 3 in ROI (2) had the highest deviations, only 31 and 18 min compared to the theoretical estimation of 3.4 and 143.7 min, respectively; in contrast, other deviations fluctuated from several tenths to 2 fold. It should be noted that all 3 ROI (1) results in model A had larger derived biological half-lives than the theoretical values, indicating that the radio-active solution remained longer in the first spherical chamber (ROI (1)) than predicted. In addition, case 1 in ROI (2) had a longer biological half-life (290 min) than theoretical one (143.7 min); however, this result was acceptable because the 3 valves around ROI (2) were preset tightly in that specific case. Therefore, the practical half-life may have been longer than predicted because of minor leakage along the ditches (see Fig. 2A).

AT examination

The scanned data from each case were analyzed and normalized to yield input data for the optimization program in MATLAB. An agreement value (AT) was used to determine the similarity between the optimal results obtained by MATLAB and the empirical data for each case. It was defined as

$$AT_{value}\% = \sqrt{\frac{\sum_{i=1}^{n}\left(\frac{Y_i(Matlab) - Y_i(nor.)}{Y_i(nor.)}\right)^2}{N}} \times 100\% \qquad (10)$$

where Y_i (nor.) and Y_i(Matlab) were the normalized intensity from each ROI determined from the n_{th} set of empirically obtained data and computed using MATLAB, respectively. The value of N was set at 19 so that every 10 min represented a point from the interpolation of the practical data set. An AT of zero implied perfect agreement between the analytical and empirical results. Generally, an AT under 15.0 could be regarded as indicating excellent consistency between the optimal computational and empirical data, while an AT between 15.0 and 30.0 supported reasonable confidence in their consistency.[12-14] Table 2 displays the ATs for the 5 cases studied. The AT indicates the curve fitting agreement between the theoretical estimation and practical measurement for every specific ROI. Interpreting the data as a feasibility study, 4 and 8 out of 20 ATs were below 15.0 and 30.0, respectively, indicating that the technique is acceptable.

Discussion

Case interpretation

Case 1 demonstrates a simple chain decay among ROIs (1), (4), and (3) according to its own effective half-life ($1/T1_{/2}$(eff) = 1/ $T_{1/2}$(R) + $T1_{/2}$(bio)).[15] The theoretical effective half- lives for ROIs (1), (4), and (3) are 24.9, 72.3, and 3.4 min, respectively. In contrast, the measured effective half-lives are 47.0, 71.0, and 7.8 min. The preset valves around ROI (2) located in ditches 12, 23, and 25 as shown in Fig. 2 model A,

Table 2. The ATs for the 5 cases studied. The AT indicates the curve fitting agreement between the theoretical estimation and practical measurement for every specific ROI.

	Model A			Model B	
	Case 1	Case 2	Case 3	Case 4	Case 5
ROI (1)	6.2	18.7	5.6	37.2	32.0
ROI (2)	28.4	18.7	41.9	45.9	23.3
ROI (3)	26.9	24.2	32.7	38.0	48.7
ROI (4)	20.1	9.2	26.3	13.1	16.5

performed only a limited function in holding the feed-water; the measured biological half-life still reached 290 min indicating a real leakage rate of 2.5 cc/min.

Case 2 demonstrates 2 independent chain decays that did not interfere with each other, according to the theoretical arrangement. As Fig. 2 shows, the valves in ditches 13 and 23 were tight. The leakage along the ditches allowed some solution to mix together and be deposited in ROI (3), extending the derived biological half-life from the theoretical 3.4 to 31 min (see Table 1).

Case 3: The only condition for optimizing the MATLAB program for case 3 was that the sum of I_{12}, I_{13}, and I_{14} needed to equal 1.00, because all of the valves were released during data acquisition. Therefore, the short biological half-life of ROI (2) might be attributable to the highest branching ratio of the infused feed-water, 0.36 compared to 0.34 and 0.30. The optimal MATLAB solutions for each case converged at a minimum AT integrated from the ATs of the 4 ROIs. Therefore, the reported data represent the compromise solution between the theoretical estimations and practical measurements.

Case 4: Model B defined the biokinetic model differently from model A, even though the 2 were easily interchangeable by simply overturning the water phantom. The complicated time-dependent, simultaneous differential equations made model B difficult to optimize in the MATLAB program. Case 4 can be treated as 2 independent paths of chain decay, from ROIs (3) and (2) to (1) and ROI (4) to (1) (see Fig. 2 Model B). The derived parameters fell under the accepted levels, although ROI (3)'s evaluated biological half-life of 18 min was higher than the predicted 3.4 min. The comparatively small volume of ROI (3) made its calculation complex. In addition, the sum of I_{25}, I_{35}, and I_{45} also equals 1.00, similar to the limitation in case 2 that made it difficult to maintain consistency in MATLAB calculations.

Case 5 presents the most complicated case of all, although the derived parameters have the highest agreement with the theoretical ones (see Table 1). The

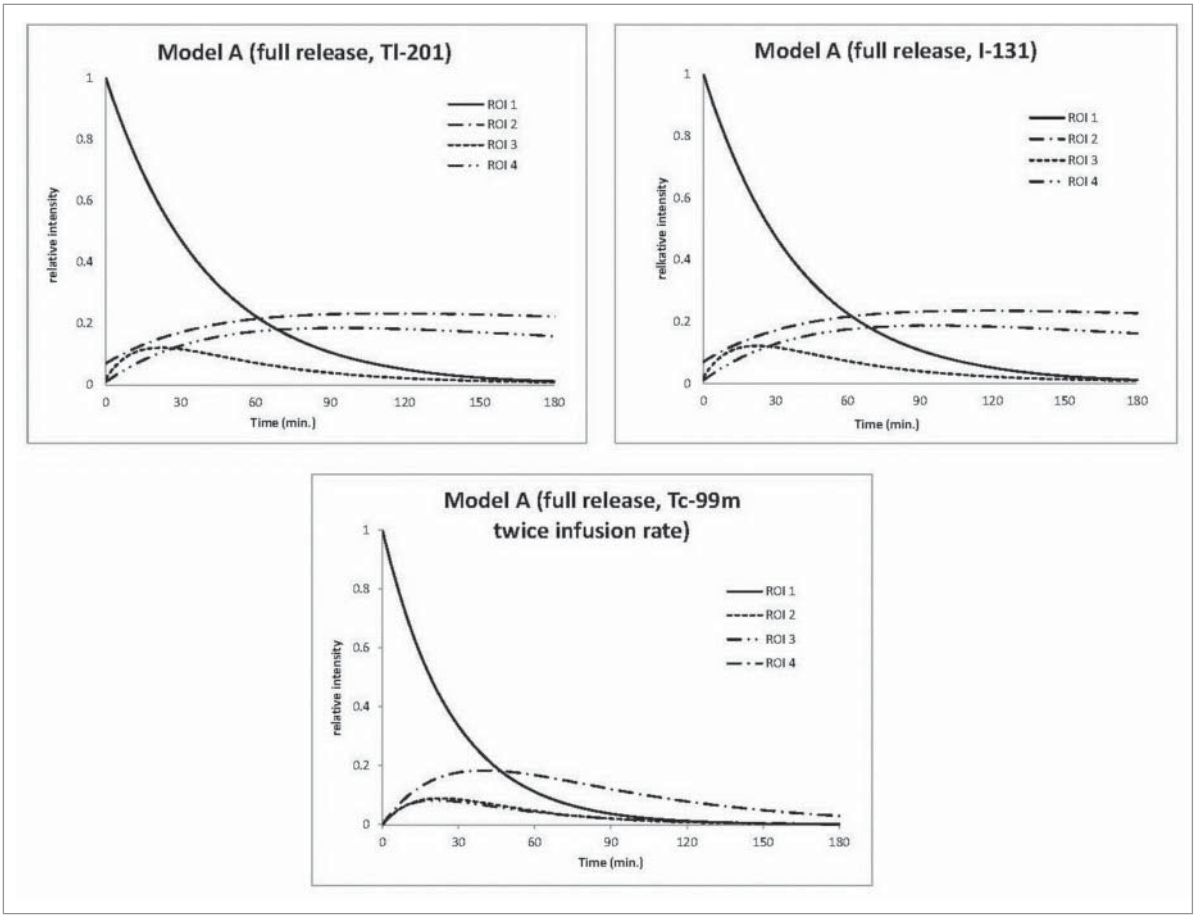

Figure 6. Three MATLAB calculation results using different settings. In the first 2 plots, Tc-99 m is replaced by Tl-201 (T1/2(R) = 3.04 d) and I-131 (T1/2(R)=8.03 d), respectively, and in the last plot, the labeled radionuclide is still Tc-99 m but the feed water infusion rate is 10 cc/min, double original rate.

characteristics of the derived lines reflect a different setting in dealing with the water phantom. Unlike model A, where ROI (1) was the first receiver to hold the infused feed-water, model B's case 5 had no buffer zone at all. The infused water divided directly between ROIs (2), (3), and (4) before collecting together in ROI (1) to drain out of the water loop (see Fig. 2). The interaction among the 4 ROIs allowed the time-dependent on-site measurement to become unpredictable, therefore, the MATLAB program could only provide theoretical estimations that needed to be verified practically in order to maintain consistency.

Replacement radionuclide solutions

The preset radionuclide TC-99 m can be replaced with any other radionuclide in the MATLAB program. This is convenient for researchers or medical professionals who wish to explore the applications of this technique toward other medical needs. Figure 6 depicts 3 MATLAB calculation results using different settings. In the first 2 plots, Tc-99 m is replaced by Tl-201 ($T_{1/2}$(R) = 3.04 d) and I-131 ($T1_{/2}$(R) = 8.03 d), respectively, and in the last plot, the labeled radionuclide is still Tc-99 m but the feed water infusion rate is 10 cc/min, double original rate. As Fig. 6 clearly illustrates, the first 2 plots perform similarly with regard to the time–dependent intensity of ROIs, because the preset biological half-life of every ROI dominates the curve characteristics. A radiological half-life of 3.04 days or 8.03 days has a negligible contribution to the time-dependent intensity change; in contrast, the biological half-life of the 4 ROIs varied from 3.4 min to 143.7 min in the original setting. When the feed water infusion rate doubles from 5 to 10 cc/min, then the predicted results become extremely different, because the radioactive degradation in ROI (1) falls at twice the preset rate. ROIs (2), (3), and (4) also change according to the cross interaction among ROIs.

Conclusion

This study analyzed multiple biokinetic models using a dynamic water phantom. Well interpreting the biokinetic models can help to evaluate internal radioactive dosage, to improve administrated dose delivery system, and to assess metabolic mechanism of the radio-nuclides labeled compound for patient undergone nuclear examination. An appropriate phantom can provide many advantages in metabolic simulation from practical viewpoint. Ultimately, the dynamic water phantom proved successful in this feasibility study in 3 ways: (1) in representing the biokinetic model that mimics the human body's metabolic mechanisms; (2) in verifying theoretical estimations from a self-developed MATLAB program; and (3) in offering many usage configurations by varying the 8 valve poles between the ROIs. Furthermore, the biokinetic models coupled with the MATLAB program are easily preset in order to fulfill different criteria and meet highly changeable needs. In addition, the quantified ATs varied from 5.6 to 48.7 over the 5 cases, indicating that this work presented an acceptable contribution.

Disclosure of potential conflicts of interest

No potential conflicts of interest were disclosed.

Funding

The authors would like to thank the Ministry of National Defense-Medical Affairs Bureau under contract No. ND 104-A04 and the Ministry of Science and Technology of the Republic of China, under contract No. MOST 103-2221-E-166-003-MY3 for financially supporting this research.

References

[1] Dynamic Cardiac Phantom™, ECT/DY-CAR/P, Available from: http://www.spect.com/pub/Dynamic_Cardiac_Phantom.pdf

[2] IEL, Imaging equipment Ltd., dynamic phantom, Available from: http://www.imagingequipment.co.uk/product/708-110/Dynamic-Phantom

[3] Killoran JH, Gerbaudo VH, Mamede M, Ionascu D, Park SJ, Berbeco R. Motion artifacts occurring at the lung/diaphragm interface using 4 D CT attenuation correction of 4 D PET scans. J Applied Clin Medical Phys 2011; 12(4):3502

[4] Isabelle CB, Irene P, Ourania D, Lefteris L, Antonis L, Antonis A, Stelios C, Charalambos Y, Demetris K, Christoforos P, et al. Characterization of attenuation and respiratory motion artifacts and their influence on SPECT MP image evaluation using a dynamic phantom assembly with variable cardiac defects. J Nuclear Cardiol 2016; 1–10; e-pub ahead of print.

[5] Dogan H, Veldkamp WJH, Dibbets-Schneider P, Spijkerboer AM, Ertens BJA, Kroft LJM, Roos ADE, Geleijns J. Effects of heart rate, filling and slice thickness on the accuracy of left ventricular volume measurements in a dynamic cardiac phantom using ECG-gated MDCT. British J Radiol 2008; 81:577–82; http://dx.doi.org/10.1259/bjr/92798700

[6] Yang J, Yamamoto T, Mazin SR, Graves EE, Keall PJ. The potential of positron emission tomography for intratreatment dynamic lung tumor tracking: A phantom study.

Medical Physics 2014; 41:021718; PMID:24506609; http://dx.doi.org/10.1118/1.4861816

[7] Luo X, Kitasaka T, Mori K. Externally Navigated Bronchoscopy Using 2-D Motion Sensors: Dynamic Phantom Validation. IEEE Transactions Medical 2013; 32(10):1745–64; http://dx.doi.org/10.1109/TMI.2013.2263152

[8] ICRP-30, Limits for intakes of radionuclides by workers. Technical Report ICRP-30, International commission on radiation protection, Pergamon Press, Oxford 1978

[9] ICRP-100, Human alimentary tract model for radiological protection. Technical Report ICRP-100. International Commission on Radiation Protection. Pergamon Press 2005

[10] IAEA, Human Health Campus, Tc-99 m MDP labelled diphosphonate. Available from: https://nucleus.iaea.org/HHW/Radiopharmacy/VirRad/Selection_of_Labelling_Kit/

[11] Knoll GF. Radiation Detection and Measurement. John Wiley and Sons, New York second edition 1989

[12] Chen CY, Chang PJ, Changlai SP, Pan LK. Effective Half Life of Iodine for Five Thyroidectomy Patients Using an in vivo Gamma Camera Approach. J Radiation Res 2007; 48(6):485–93; http://dx.doi.org/10.1269/jrr.07031

[13] Chen CY, Pan LK. Trace elements of Taiwanese dioscorea spp. Using instrumental neutron activation analysis. Food Chem 2001; 72:255–60; http://dx.doi.org/10.1016/S0308-8146(00)00241-7

[14] Hsu CC, Chen PY, Chen CC, Pan LK. Measurement of gastric emptying time of solids in healthy subjects using scintigraphic method: a revised technique. Radiation Protection Dosimetry 2012; 150:405–14; PMID:22090418; http://dx.doi.org/10.1093/rpd/ncr425

[15] Turner JE. Atoms, Radiation, and Radiation Protection, second ed. John Wiley & Sons, Inc. 2000. ISBN 978-3-527-40606-7